Graphene oxide–P25 photocatalysts for degradation of diphenhydramine pharmaceutical and methyl orange dye

Sergio Morales-Torres, Luisa M. Pastrana-Martínez, José L. Figueiredo, Joaquim L. Faria, Adrián M.T. Silva*

LCM – Laboratory of Catalysis and Materials – Associate Laboratory LSRE/LCM, Faculdade de Engenharia, Universidade do Porto, Rua Dr. Roberto Frias, 4200-465 Porto, Portugal. Fax: +351-22-5081449; Tel: +351-22-5081582.

*Corresponding author e-mail address: adrian@fe.up.pt (A.M.T. Silva)

Abstract

Graphene oxide (GO) and the benchmark TiO_2 photocatalyst (P25) were used to prepare different composites (GOP), by a simple method of mixing and sonication, varying the GO content and the heat-treatment temperature under nitrogen. The composites were characterized by thermogravimetric (TG) and differential thermogravimetric (DTG) analyses, scanning electron microscopy (SEM), physical adsorption of nitrogen, diffuse reflectance UV-Vis (DRUV) and IR (DRIFT) spectroscopies, and point of zero charge (pH_{PZC}) measurements. The morphology, microporosity and S_{BET} of the composites did not vary significantly in comparison to P25, while an increase of their mesoporosity and mesopore diameter were observed due to the formation of GO aggregates coated with P25 nanoparticles. The aggregates were stabilized by the formation of Ti-O-C bonds, which in turn produced a narrowing of the band gap relative to P25. The surface chemistry of GOP composites varied with the GO content, being more acidic when higher GO content was used. The photocatalytic performance was evaluated for the degradation of diphenhydramine (DP) pharmaceutical and methyl orange (MO) dye under near-UV/Vis irradiation. The first order rate constant of MO photodegradation increased four times for some GOP composites with relation to P25 (i.e., from $k = 52\times10^{-3}$ to 207×10^{-3} min^{-1}). Comparable efficiencies were observed when DP was used as model pollutant (i.e., around $k = 54\times10^{-3}$ min^{-1}). The best performing photocatalyst was that containing 1.4 wt.% GO and treated at 200-300 ºC. The improved performance was attributed to the reduction of GO during the thermal treatment and to the good contact between the TiO_2 and the carbon phases.

Keywords: *graphene oxide, P25, composite, diphenhydramine, methyl orange.*

1. Introduction

Availability of enough quality water is an important issue in large and industrialized cities as well as in less developed regions. For this reason the adequate treatment of industrial and household effluents is an active field of research. In the recent years, advanced oxidation processes (AOPs), which are based on the oxidation of pollutants by highly oxidizing radicals (such as hydroxyl radicals), have gained major attention. In particular, heterogeneous photocatalysis is one of the most promising AOPs, the generation of electron/hole pairs in the photocatalyst, when exposed to light irradiation, inducing complete mineralization of persistent pollutants. TiO_2 is the most studied photocatalyst for water purification and wastewater treatment, due to its inert nature, biocompatibility, low cost and high chemical stability [1]. In spite of its excellent photocatalytic properties, compared with other semiconductors, there is a large effort for the sake of improving its activity under near-UV/Vis irradiation, aiming at solar applications [2].

Nanostructured carbon materials (e.g. fullerenes (C_{60}), carbon nanotubes (CNT) and graphene) have recently gained significant attention, particularly graphene, due to its specific properties, including large specific surface area, flexible structure, excellent mobility of charge carriers and good electrical and thermal conductivities [3]. These properties are important features when dealing with the preparation and use of graphene-based materials and, for this reason, graphene-based TiO_2 composites are being developed and successfully applied as photocatalysts for the treatment of pollutants and for the prevention of microorganisms in both water and air [4-7].

Recently, we have prepared different graphene oxide-TiO_2 composites using ammonium hexafluorotitanate as TiO_2 precursor and the liquid phase deposition method [8]. It was concluded that the optimum GO content and treatment temperature were 3.3-4.0 wt.% and 200 ºC, respectively, these conditions yielding composites with higher photocatalytic performance than P25 in the photodegradation of diphenhydramine (DP) pharmaceutical and

methyl orange (MO) dye under both near-UV/Vis and visible irradiation. In addition, we have used other nanostructured carbon materials, such as carbon nanotubes and fullerenes, to prepare composites with the same kind of TiO_2 precursor, the photocatalytic performance depending on the nature and content of the carbon phase and the higher photocatalytic activity for DP and MO degradation being usually obtained with composites prepared with GO [9].

In the present study the composites with GO were prepared using the well-known reference TiO_2 photocatalyst from Evonik/Degussa (P25), the resulting composites being hereafter labelled as GOP. These GOP composites were prepared by a simple mixing and sonication method and using a thermal post-treatment under nitrogen, the GO content and the temperature of treatment being optimized. The photocatalytic performance of these new materials was tested against the benchmark standard P25 on the photodegradation of DP and MO under near-UV/Vis irradiation.

2. Materials and methods

2.1. Preparation of GO and GOP composites

For the synthesis of GO, natural graphite (99.9995% purity from Sigma-Aldrich) was oxidized by the modified Hummers method [10], by means of strong oxidizing agents ($KMnO_4$, $NaNO_3$) in acidic media (H_2SO_4). After that, the material obtained was repeatedly washed with water and finally sonicated in an immersion bath (UP400S, 24 kHz) for 1 h. The final sonicated dispersion was centrifuged at 3000 r.p.m. for 20 min and the non-exfoliated graphite oxide removed, resulting in a pure GO aqueous dispersion.

GOP composites were prepared by simple mixing and sonication. Briefly, ethanol was added to the GO aqueous dispersion in a proportion of 1:2, respectively, and then 1 g of P25 (supplied from Degussa Co., Ltd., Germany, now Evonik) was added under vigorous stirring. The obtained suspension was left to rest for 30 min at room temperature. After that, the

suspension was sonicated for 1 h in an immersion bath, yielding a homogeneous grey suspension, which was filtered using a GN-6 Metricel® MCE (Pall Corporation). The recovered material was washed with water, and dried overnight at 110 ºC under vacuum. The obtained GOP composites were milled and sieved (particles < 100 μm) prior to their use in characterization and photocatalytic experiments. In addition, some selected composites were finally subjected to a thermal treatment (see temperatures in the following) under nitrogen.

Different amounts of GO (1.0, 1.4, 2.9, 3.3, 6.0 wt.%) and treatment temperatures (200, 300 and 450 °C) were tested. GOP composites will be denoted as GOP-X-Y, where X and Y are the GO wt.% and the thermal treatment temperature, respectively. It is known that thermal treatments of GO under inert atmosphere are used to reduce GO in order to obtain reduced graphene oxide (RGO), by the partial removal of oxygenated groups anchored in the GO structure; thus some partial reduction of GO may take place under the conditions used by us.

2.2. Characterization techniques

The morphology of the materials was studied by scanning electron microscopy (SEM) using a FEI Quanta 400FEG ESEM/EDAX Genesis X4M microscope. Textural characterization of the samples was carried out by N_2 adsorption–desorption at −196 ºC with a Quantachrome NOVA 4200e apparatus. The Brunauer–Emmett–Teller (BET) [11] and Dubinin–Radushkevich [12] equations were applied to determine the apparent surface area (S_{BET}) and the micropore volume (V_{micro}), respectively. The BJH method [13] was applied to the desorption branch of the N_2 isotherms to determine the pore size distribution, the average mesopore diameter (d_{pore}) and volume (V_{meso}). This method was only applied for comparison between the samples and taking into account that its application is more appropriate for adsorption isotherms of type- IV according to IUPAC classification [14].

The surface chemistry of the materials was analyzed by diffuse reflectance infrared Fourier transform (DRIFT) spectroscopy and point of zero charge (pH_{PZC}) measurements. DRIFT spectra were recorded on a NICOLET 510P FTIR spectrometer equipped with a beam collector (Spectra Tech). The pH_{PZC} was determined following a previously published methodology [15], and corresponds to the equilibrium pH for 100 mg of the material dispersed in 2 mL of water (at 25 ºC).

Thermogravimetric (TG) and differential thermogravimetric (DTG) analyses of GOP composites were performed by heating the sample in air or nitrogen flow from 50 ºC to 900 ºC at 20 ºC min^{-1} using a STA 490 PC/4/H Luxx Netzsch thermal analyser. The GO content (wt.%) in a given composite was estimated by subtracting the weight loss obtained with P25 under air atmosphere (oxidizing conditions) from the weight loss obtained with the composite. In addition, the percentage of RGO was estimated taking into account the weight loss of the composite at a given temperature (200, 300 and 450 ºC) with respect to the total weight loss of the composite when heated up to 900 ºC, both under nitrogen atmosphere (inert conditions).

The optical properties of the samples were analyzed by UV/Vis diffuse reflectance (DRUV) spectroscopy using a JASCO V-560 UV/Vis spectrophotometer, equipped with an integrating sphere attachment (JASCO ISV-469). Barium sulfate ($BaSO_4$) was used as a reference. The reflectance spectra were converted to equivalent absorption Kubelka-Munk units by the instrument software (JASCO). The band gap was determined from the plots of transformed Kubelka-Munk as a function of the energy.

2.3. Photocatalytic experiments

The photocatalytic efficiencies of the materials were evaluated for DP (3.40×10^{-4} mol L^{-1}) and MO (3.05×10^{-5} mol L^{-1}) removal in aqueous media under near-UV/Vis irradiation, as

described elsewhere [8,16]. The amount of P25 was kept at the optimal values of 1.0 g L^{-1} and 0.5 g L^{-1} for DP and MO, respectively, not only in experiments with P25 but also in those performed with GOP composites, i.e. maintaining the same amount of P25 in all performed experiments regardless the GO content used. Reaction in the absence of catalyst and under the same experimental conditions was performed as a blank experiment for both pollutants. The concentration of DP was determined by HPLC with a Hitachi Elite LaChrom system equipped with a Hydrosphere C18 column, a Diode Array Detector (L-2450) and a solvent delivery pump (L-2130). An isocratic method (flow rate of 1 mL min^{-1}) was used with the eluent consisting of an A:B (70:30) mixture of 20 mM NaH_2PO_4 acidified with H_3PO_4 at pH = 2.80 (A) and acetonitrile (B). The absorbance was found to be linear over the whole range considered. The concentration of MO was determined by UV-Vis spectrophotometry at 464 nm in a Jasco V-560 spectrophotometer. The total organic carbon (TOC) was also determined for selected samples using a Shimadzu TOC-5000A analyzer. The maximum relative standard deviation of both HPLC and TOC measurements was never larger than 2%.

The experiments revealed that the photocatalytic oxidation of the studied pollutants can be described by a pseudo-first order kinetic model, according to the following equation:

$$C = C_0 e^{-kt} \quad (1)$$

where C corresponds to pollutant concentration, k is the pseudo-first order kinetic constant, t is the reaction time, and C_0 is the pollutant concentration at t = 0 min. For comparison, all the experimental conditions used in this work, as well as the respective k constants obtained by fitting Eq. (1) to the normalized pollutant concentration histories (C/C_0). The Marquardt–Levenberg algorithm used seeks the values of the parameters that minimize the sum of the squared differences between observed and predicted values of the dependent variable (the tolerance was set at 1×10^{-10}). The regression coefficient (r^2) was used to assess the quality of the fitting.

3. Results and discussion

3.1. Characterization of the photocatalysts

The SEM micrographs of P25 particles are shown in Figures 1a and b for two different magnifications. Regarding the GOP composites (Figures 1c-h), most of them presented a homogeneous morphology composed by GO layers coated by joined nanoparticles of P25. However, when the highest GO content was used (GOP-6.0), some GO nanosheets remained uncoated with P25 nanoparticles (Figure 1h). In general, this loss of good assembly between both phases was also observed for composites treated under nitrogen at 450 ºC, while those prepared at lower temperature (200 and 300 ºC) maintained a good contact between both phases (e.g., GOP-1.4-200 in Figure 1e). The EDX spectra obtained for the GOP composites (as shown in Figure 1i for GOP-6.0) revealed Ti, O and C peaks, that were associated to TiO_2 in P25 and to GO (the O peak resulting from TiO_2 and from the oxygenated surface groups present in the chemical structure of GO). Therefore, the method of simple mixing and sonication used in the preparation of GOP composites in general leads to a good contact between P25 nanoparticles and GO nanosheets, as previously observed by Zhang et al. [17].

Regarding the textural characterization, Figure 2 shows the N_2 adsorption-desorption isotherms for some GOP composites and P25. In general, all isotherms showed an adsorptive behaviour of type-II, in accordance with IUPAC classification, characteristic of macroporous materials or of materials presenting low porosity [14]. In addition, they also presented a small hysteresis loop of type H3, typical of aggregates formed by plate particles or adsorbents with slit-shaped pores, which could correspond to GO layers coated with P25 nanoparticles, as clearly observed in the SEM image shown in Figure 1g. A poor effect on the microporosity (V_{micro}) and S_{BET} was observed when GO was added to P25 (Table 1), the resulting composites presenting similar values to those measured for P25 (e.g., for GOP-1.4 and P25 the same S_{BET}

and V_{micro} were determined, 55 m^2 g^{-1} and 0.02 cm^3 g^{-1}, respectively) or slightly higher values when higher GO contents were used (e.g., GOP-3.3 and GOP-6.0). These observations are in agreement with other works [17,18] and could be explained because the method of preparation used induces only small changes on the original microporosity of P25. In spite of the small S_{BET} developed, significant changes were produced on the mesoporosity and pore size distribution of all samples, a mesopore volume twice higher than that measured for P25 being obtained (e.g., 0.44 cm^3 g^{-1} for GOP-6.0 in comparison with 0.20 cm^3 g^{-1} for P25). The formation of GO aggregates coated with P25 nanoparticles not only had an effect on the mesopore volume but also on the diameter of the mesopores, wider pores being obtained for the composites than for P25. For instance, P25 presented a broad mono-modal pore size distribution with an average pore diameter around 29.8 nm, while the average pore diameter for most of the composites was around 32.8-33.2 nm, due to the dispersion of P25 nanoparticles on both sides of GO layers. On the other hand, the post-treatment performed at different temperatures had poor effect on the porosity of the corresponding GOP composites, which could be explained again by the method of preparation and the low original porosity of P25, since GO-TiO_2 composites previously prepared by us (using the liquid phase deposition method and ammonium hexafluorotitanate as TiO_2 precursor) presented lower microporosity and higher mesoporosity after the N_2 post-treatment at high temperature [8].

DRIFT analysis was used to study the possible interactions between TiO_2 and carbon phases. Figure 3 shows the DRIFT spectra for P25, GO and also for GOP-6.0 before and after N_2 treatment at 200 ºC. The DRIFT spectrum recorded for P25 showed mainly a broad band situated at 400-800 cm^{-1}, which corresponds to the vibration of Ti-O-Ti bonds present in the structure of P25 [19]. In addition, other broad band of lower intensity was observed at 3264 cm^{-1}, associated with the stretching vibration of water molecules and confirmed with a small peak centred at 1600 cm^{-1}, although the presence of Ti-OH bonds could also have certain contribution

to this peak [19]. For GOP-6.0 and GOP-6.0-200 composites, significant differences were found in comparison with P25. For instance, the band corresponding to the vibration of Ti-O-Ti bonds was shifted towards higher wavenumber (889 cm^{-1}), which was explained by Zhang et al. [18] by the possible formation of Ti-O-C bonds. However, due to the overlapping of bands below 1000 cm^{-1}, it is more appropriate to corroborate the formation of these Ti-O-C bonds by looking at the band centred at 1261 cm^{-1} [20], which appeared for the GOP composite and was not observed for P25. These bands could be originated from hydroxy groups of P25 and some oxygenated groups of GO (e.g. carboxylic groups), which can be observed in the spectra of both GO and GOP materials (band at 1710 cm^{-1} related to the stretching vibration of C=O bonds [21]). In the case of GO, a broad band situated between 1020-1394 cm^{-1} was attributed to the overlapping of the bands corresponding to the tertiary C-OH and C-O stretching [22]. On the other hand, GOP composites presented a band of skeletal vibration at 1560 cm^{-1}, typical of graphene sheets [23], which was larger in the case of GOP-6.0-200 due to the removal of some oxygenated groups and the formation of RGO.

The surface chemistry of the materials was also characterized by pH_{PZC} measurements and the values are collected in Table 1. As previously verified by DRIFT analysis, the surface chemistries of P25 and GOP composites were very different. P25 has a nearly neutral pH_{PZC} (6.3), while all GOP composites presented more acidic characteristics due to the addition of GO that has a large amount of oxygenated groups. The pH_{PZC} decreased with the increase of the GO content as follows: 4.1 > 4.0 > 3.5 > 3.2 > 3.0 for GOP-1.0, GOP-1.4, GOP-2.9, GOP-3.3 and GOP-6.0, respectively. On the other hand, the post-treatment performed at different temperatures modified also the surface chemistry of GOP composites, leading to the formation of RGO and, as consequence, to materials with less acidic properties due to the partial removal of the acid groups; namely, the pH_{PZC} increased with the temperature of treatment as follows:

3.2 < 3.5 < 3.9 < 4.5 for GOP-3.3 before and after treatment at 200, 300 and 450 ºC, respectively.

In addition, the RGO content after the thermal treatment depends not only on the temperature used but also on the GO content. For instance, the percentages of RGO obtained for GOP-3.3 were 13, 28 and 54% when the material was treated at 200, 300 and 450 ºC, respectively. The percentage determined for pure GO at a given temperature was always higher, namely 19, 51 and 68% at 200, 300 and 450 ºC, respectively. This indicates that some oxygenated groups in the GOP composites could be associated to P25 nanoparticles, by means of Ti-C-O bonds, preventing their removal during the thermal treatment.

Finally, the optical properties of the GOP composites were analysed using DRUV spectroscopy, these results being shown in Figure 4a. All composites presented higher light absorption intensities than P25, in particular for the visible region of the spectra. This effect was also verified for other carbon-TiO_2 composites [24], including those prepared with graphene [4,8,25], which presented larger light absorption intensity in visible region by increasing the GO content, as also observed in Figure 4a. Although the determination of band gaps is difficult due to the significant increase of the background absorption above 400 nm, the transformed Kubelka-Munk function was plotted as a function of the energy of light as shown in Figure 4b. From it, the band gaps were estimated, values of 2.54, 2.65, 2.69, 2.87, 2.88 and 3.14 eV being obtained for GOP-6.0, GOP-3.3, GOP-2.9, GOP-1.4, GOP-1.0 and P25, respectively. In all cases, narrower band gaps were obtained for the composites in comparison to P25, which can be explained by the formation of Ti-O-C bonds, as previously suggested from the other characterization techniques. In addition, a rough correlation was obtained between the band gaps and the GO content (Figure 4b, inset), which could be related with the amount of Ti-O-C bonds formed [26]; by increasing the GO content, more oxygenated surface groups are available and can be associated with P25 nanoparticles.

3.2. Photocatalytic experiments

3.2.1. DP photocatalytic degradation

The composites obtained with different GO contents and treatment temperatures, as well as P25, were evaluated in the photodegradation of DP under near-UV/Vis irradiation (Figure 5a-b). The respective pseudo-first order rate constants are shown in Table 2. Firstly, DP is a very resistant pollutant in the absence of a catalyst, since the conversion observed is less than 6% in 60 min (Figure 5a). The adsorption capability of the GOP composites was also determined under dark experiments, being around 5% and 8% for GOP-1.0 and GOP-6.0, respectively, which are the composites with the lowest and highest GO content.

The photocatalytic activity of the prepared materials for DP degradation follows the sequence (Figure 5a and Table 2): P25 (56×10^{-3} min^{-1}) > GOP-1.4 (46×10^{-3} min^{-1}) > GOP-1.0 (41×10^{-3} min^{-1}) > GOP-2.9 (29.7×10^{-3} min^{-1}) > GOP-3.3 (24.6×10^{-3} min^{-1}) > GOP-6.0 (18×10^{-3} min^{-1}), where the values in brackets refer to the pseudo-first order rate constants.

The results indicate that GOP composites were less active than P25 for DP degradation (Figure 5a), although their activity depended on the GO content. Figure 5a shows a clear increase in the pseudo-first order rate constants for DP degradation, from 18×10^{-3} to 46×10^{-3} min^{-1}, related with the decrease in the GO content, from 6.0 to 1.4 wt.%, respectively. Thus, among the GOP composites tested, the highest pseudo-first order rate constant was obtained for that prepared with a GO content of 1.4 wt.% (46×10^{-3} min^{-1}).

Regarding the associated mineralization, Figure 6 shows the TOC removals after 60 min for the non-catalytic experiment, for P25 and for the GOP composites prepared with three different GO contents (1.4, 3.3 and 6.0 wt.%). In general, the TOC reduction follows the similar trend observed for DP conversion (Figure 5a): GOP-1.4 produced a TOC removal of 50% while TOC reductions of 34% and 21% were observed for GOP-3.3 and GOP-6.0, respectively. It is

also noteworthy to refer that the mineralization levels of GOP-1.4 and P25 were quite similar (TOC removals of 50% and 48%, respectively). Therefore, the performances of GOP-1.4 and P25 in terms of TOC removals are comparable at such conditions, being observed that the activity of GOP-1.4 for the TOC removal is even slightly higher than that of P25.

Subsequently, the effect of the treatment temperature on the photocatalytic activities of the composites was evaluated for DP degradation. Figure 5b shows the results obtained with the composites prepared with 1.4 and 3.3 wt.% of GO content and when the thermal treatment was performed at 200, 300, and 450 ºC to these composites, namely: GOP-1.4-200, GOP-3.3-200, GOP-3.3-300 and GOP-3.3-450. The photocatalytic activity of GOP-3.3 was influenced with the calcination temperature, increasing in the case of 200 and 300 ºC but decreasing for 450 ºC (i.e., 24.6×10^{-3}, 27.9×10^{-3}, 31.4×10^{-3} and 20×10^{-3} min^{-1} for GOP-3.3, GOP-3.3-200, GOP-3.3-300 and GOP-3.3-450, respectively, Table 2). This photocatalytic behavior should be related with the increase of RGO content in the composites, which has a higher conductivity than GO [27]. However, the good contact between P25 nanoparticles and GO layers by means of Ti-O-C bonds is also crucial and could explain the decrease of efficiency when the nitrogen post-treatment was performed at 450 ºC. Taking into account that lower temperatures of treatment are favourable for the photocatalytic activity and that the optimal temperature of treatment in previous works was 200 ºC [8,9], the temperature of 200 ºC was selected for the thermal treatment of the best untreated GOP composite (i.e. GOP-1.4). Once again, the photocatalytic activity was increased by using the thermal treatment with nitrogen (from 46×10^{-3} to 54×10^{-3} min^{-1} with GOP-1.4 and GOP-1.4-200, respectively). In fact, the pseudo-first order rate constant obtained with GOP-1.4-200 was similar to that obtained with P25 (56×10^{-3} min^{-1}).

In our previous study using ammonium hexafluorotitanate as TiO_2 precursor and the liquid phase deposition method [8], different temperatures of treatment were also studied. The

highest efficiency was also obtained for a composite calcined at 200 ºC (prepared with a GO content of 3.3-4.0 wt.%), the high efficiency being attributed to the improvement of the GO conductivity as well as to the enhancement of the electronic coupling of the GO sheets with the TiO_2 nanoparticles, evidenced by the reduction of the corresponding photoluminiscence emission. As shown in the present study, the optimal GO content is lower when using P25 (1.4 wt.%) instead of TiO_2 prepared with ammonium hexafluorotitanate (3.3-4.0 wt.%), but both temperature of treatment and GO content are also important parameters when P25 is used to prepare composite materials with good photocatalytic performances.

3.2.2. MO photocatalytic degradation

The photocatalytic activity of P25 and different GOP composites was also evaluated for the degradation of an azo dye, MO, under near-UV/Vis irradiation (as shown in Figures 7a and b). The kinetics of the process are presented in Table 2. Figure 7a shows that MO is very resistant to photodegradation in the absence of a catalyst (3% of MO conversion in 30 min). The photocatalytic efficiency of the prepared materials for MO degradation was found as: GOP-1.4 > GOP-1.0 > GOP-2.9 > GOP-3.3 > GOP-6.0 > P25. The results indicate that any content of GO in the GOP composite leads to higher pseudo-first order rate constants for MO conversion (up to 138×10^{-3} min^{-1} for GOP-1.4) in comparison to bare P25 (52×10^{-3} min^{-1}). In addition, the composite prepared with an amount of GO equal to 1.4 wt.% exhibited the highest pseudo first order rate constant for MO conversion, as observed when DP was used as model pollutant. In fact, the pseudo first order rate constant obtained for GOP-1.4 is two times higher than that determined for P25. Regarding the respective MO mineralization, the TOC reduction was also determined for the photocatalytic experiments performed with different composites, the same tendency being observed for MO mineralization and degradation; i.e., GOP-1.4, GOP-

3.3 and GOP-6.0 catalysts produced after 30 min a TOC reduction of 52%, 48% and 46%, respectively, while P25 leads to a TOC reduction of 45% (Figure 6).

Zhang et al. [4] prepared also GOP composites with different GO contents, but using the hydrothermal method, that were also tested in the photocatalytic degradation of MO under UV/Vis irradiation. These authors concluded that the optimum GO content was 5 wt.%, although the GOP composite with 1-2 wt.% GO content was also very active. In the present work the optimal amount of GO was lower than in the work of Zhang et al. (i.e., 1.4 wt.% instead of 5 wt.%, respectively). This could occur because the preparation methods are different and the amounts of RGO, that are not indicated in the work presented by Zhang et al. and that have influence on the photocatalytic activity of the resulting composites (as previously demonstrated in the present work), could be also different.

Figure 7b shows the results obtained with the most active composite (GOP-1.4) treated at 200 ºC and 300 ºC. Once again, it was found that the photocatalytic activity increases when the material is treated at 200-300 ºC. In addition, all GOP composites present higher photocatalytic activity than P25 for MO conversion and mineralization (Figures 7a and 6, respectively). These results provide firm evidence for the beneficial effect of combining GO with P25 for the photocatalytic degradation of water pollutants and, in particular, for azo dyes. This catalytic performance could be related with the composite structure, i.e. with the formation of GO aggregates coated with P25 nanoparticles, and stabilized with the formation of Ti-O-C bonds between hydroxy groups of P25 and the oxygenated surface groups of GO. This would obviously affect the interfacial charge transfer process that can effectively inhibit electron–hole recombination [6,28].

4. Conclusions

In the photocatalytic degradation of DP and MO under near-UV/Vis irradiation, GOP-1.4 was the most active material. Above 1.4 wt.% of GO content the catalytic activity for the degradation and mineralization of both pollutants decreased with the GO content.

In addition, GOP-1.4 was more active than P25 for MO photodegradation ($k = 138\times10^{-3}$ and 52×10^{-3} min^{-1}, respectively) while for DP degradation the activity was comparable ($k = 46\times10^{-3}$ and 56×10^{-3} min^{-1}, respectively).

The thermal treatment performed on GOP composites at 200-300 ºC had a beneficial effect on the photocatalytic performance, leading to higher rate constants of photocatalytic degradation, both for DP ($k = 46\times10^{-3}$ and 54×10^{-3} min^{-1} for GOP-1.4 and GOP-1.4-200, respectively) and MO ($k = 138\times10^{-3}$ and 207×10^{-3} min^{-1} for GOP-1.4 and GOP-1.4-200, respectively). These photocatalytic activities obtained with GOP-1.4-200 are comparable or higher than those for P25, namely $k = 56\times10^{-3}$ and 52×10^{-3} min^{-1} for DP and MO degradation, respectively. Mineralization followed the same trend in all cases.

Morphology and the microporosity of GOP composites with low GO contents were comparable to those found for P25.

Mesoporosity was larger and the pore size distribution was always shifted towards wider mesoporos, whenever GO was added to P25, because P25 nanoparticles are dispersed on both sides of GO aggregates.

GOP composites possess narrower band gaps in comparison to P25. This is a consequence of the contact between TiO_2 and carbon phases being improved by the formation of Ti-O-C bonds that are probably established between the hydroxy groups of P25 and the oxygenated surface groups of GO.

The surface chemistry of GOP composites varied significantly with the GO content, more acidic materials being obtained with higher GO content.

The described results demonstrate the potential of GO to blend the benchmark P25 material and produce composites more effective in the photocatalytic treatment of waste waters, in particular those polluted with dyes.

Acknowledgments

Financial support for this work was provided by the European Commission (Clean Water - Grant Agreement nº 227017), and partially by projects PTDC/AAC-AMB/122312/2010 and PEst-C/EQB/LA0020/2011 financed by FEDER through COMPETE and by FCT - Fundação para a Ciência e a Tecnologia. SMT acknowledges financial support from SFRH/BPD/74239/2010 and AMTS from POCI/N010/2006 and PEst-C/EQB/LA0020/2011.

References

[1] R. Leary, A. Westwood, Carbon 49 (2011) 741.

[2] J. Yang, H. Bai, X. Tan, J. Lian, Appl. Surf. Sci. 253 (2006) 1988.

[3] B.F. Machado, P. Serp, Catal. Sci. Technol. 2 (2012) 54.

[4] Y. Zhang, Z.R. Tang, X. Fu, Y.J. Xu, ACS Nano 4 (2010) 7303.

[5] G. Williams, B. Seger, P.V. Kamt, ACS Nano 2 (2008) 1487.

[6] S. Morales-Torres, L. Pastrana-Martínez, J.L. Figueiredo, J.J. Faria, A.M.T. Silva, Environ. Sci. Pollut. Res., http://dx.doi.org/10.1007/s11356-012-0939-4, *in press*

[7] G. Jiang, Z. Lin, C. Chen, L. Zhu, Q. Chang, N. Wang, W. Wei, H. Tang, Carbon 49 (2011) 2693.

[8] L.M. Pastrana-Martínez, S. Morales-Torres, V. Likodimos, J.L. Figueiredo, J.L. Faria, P. Falaras, A.M.T. Silva, Appl. Catal. B 123-124 (2012) 241.

[9] L.M. Pastrana-Martínez, S. Morales-Torres, J.L. Figueiredo, J.L. Faria, A.M.T. Silva, *under review*.

[10] J. Hummers, R.E. Offeman, J. Am. Chem. Soc. 80 (1958) 1339.

[11] S. Brunauer, P.H. Emmet, E. Teller, J. Am. Chem. Soc. 60 (1938) 309.

[12] F. Stoeckli, Characterization of microporous carbons by adsorption and immersion techniques, in: J.W. Patrick (Ed.), Porosity in carbons: characterization and applications, Edward Arnold, London, 1995.

[13] E.P. Barrett, L.G. Joyner, P.P. Halenda, J. Am. Chem. Soc. 73 (1951) 373.

[14] R.C. Bansal, J.B. Donnet, F. Stoeckli, Active Carbon, Marcel Dekker, New York, 1988.

[15] C. Moreno-Castilla, F. Carrasco-Marín, C. Parejo-Pérez, M.V. Lopez Ramón, Carbon 39 (2001) 869.

[16] L.M. Pastrana-Martínez, J.L. Faria, J.M. Doña-Rodríguez, C. Fernández-Rodríguez, A.M.T. Silva, Appl. Catal. B 113-114 (2012) 221.

[17] Y. Zhang, C. Pan, J. Mater. Sci. 46 (2011) 2622.

[18] H. Zhang, X. Lv, Y. Li, Y. Wang, J. Li, ACS Nano 4 (2010) 380.

[19] S.S. Mali, P.S. Shinde, C.A. Betty, P.N. Bhosale, W.J. Lee, P.S. Patil, Appl. Surf. Sci. 257 (2011) 9737.

[20] P. Lei, F. Wang, X. Gao, Y. Ding, S. Zhang, J. Zhao, S. Liu, M. Yang, J. Hazard. Mater. 227-228 (2012) 185.

[21] J.L. Figueiredo, M.F.R. Pereira, M.M.A. Freitas, J.J.M. Orfão, Carbon 37 (1999) 1379.

[22] X. Zhou, T. Shi, Appl. Surf. Sci. 254 (2012) 566.

[23] C. Nethravathi, M. Rajamathi, Carbon 46 (2008) 1994.

[24] C.G. Silva, J.L. Faria, Appl. Catal. B 101 (2010) 81.

[25] W. Fan, Q. Lai, Q. Zhang, Y. Wang, J. Phys. Chem. C 115 (2011) 10694.

[26] Y. Min, K. Zhang, L. Chen, Y. Chen, Y. Zhang, Synth. Met. 162 (2012) 827.

[27] H.A. Becerril, J. Mao, Z. Liu, R.M. Stoltenberg, Z. Bao, Y. Chen, ACS Nano 2 (2008) 463.

[28] T.D. Nguyen-Phan, V.H. Pham, E.W. Shin, H.D. Pham, S. Kim, J.S. Chung, E.J. Kim, S.H. Hur, Chem. Eng. J. 170 (2011) 226.

TABLES

Table 1. Textural characterization and pH_{PZC} for P25 and GOP composites.

Catalysts	S_{BET} (±5 m^2 g^{-1})	V_{micro} (±0.01 cm^3 g^{-1})	V_{meso} (±0.02 cm^3 g^{-1})	d_{pore} (±0.5 nm)	pH_{PZC} (± 0.1)
P25	55	0.02	0.20	29.8	6.3
GOP-1.0	46	0.02	0.42	32.9	4.1
GOP-1.4	55	0.02	0.40	33.2	4.0
GOP-2.9	56	0.02	0.35	32.8	3.5
GOP-3.3	69	0.03	0.34	32.9	3.2
GOP-3.3-200	59	0.03	0.34	32.8	3.5
GOP-3.3-300	62	0.03	0.34	33.0	3.9
GOP-3.3-450	61	0.03	0.34	32.8	4.5
GOP-6.0	59	0.03	0.44	31.4	3.0

Table 2. Pseudo-first order kinetic rate constant (k) of DP and MO degradation under near-UV/Vis and respective coefficient of variation (CV), expressed as a percentage (k_{CV}) and regression coefficient (r^2).

Catalyst	Diphenhydramine (DP)		Methyl orange (MO)	
	k (10^{-3}min^{-1})	r^2	k (10^{-3}min^{-1})	r^2
GOP-1.0	41 ± 1	0.998	116 ± 3	0.998
GOP-1.4	46 ± 2	0.996	138 ± 4	0.997
GOP-2.9	29.7 ± 0.5	0.999	97 ± 4	0.998
GOP-3.3	24.6 ± 0.6	0.999	85 ± 2	0.998
GOP-6.0	18 ± 1	0.992	67 ± 2	0.997
GOP-1.4-200	54 ± 3	0.995	207 ± 2	0.9998
GOP-1.4-300	n.d.	n.d.	185 ± 5	0.9992
GOP-3.3-200	27.9 ± 0.7	0.998	n.d.	n.d.
GOP-3.3-300	31.4 ± 0.8	0.998	n.d.	n.d.
GOP-3.3-450	20 ± 1	0.993	n.d.	n.d.
P25	56 ± 4	0.998	52 ± 5	0.99
None (blank)	1.00 ± 0.07	0.9	1.0 ± 0.2	0.9

n.d.: Not determined

FIGURE CAPTIONS

Figure 1. SEM micrographs for (a,b) P25, (c,d) GOP-1.4, (e) GOP-1.4-200, (f) GOP-3.3, (g,h) GOP-6.0 and (i) EDX spectrum for GOP-6.0.

Figure 2. N_2 adsorption-desorption isotherms at – 196 ºC for P25, GOP-1.0, GOP-3.3 and GOP-6.0.

Figure 3. DRIFT spectra for P25, GO, GOP-6.0 and GOP-6.0-200.

Figure 4. DRUV spectra of P25 and GOP composites without thermal treatment (a), plot of transformed Kubelka-Munk as a function of the energy of light (b) and correlation between band gap energy and GO content (b, inset).

Figure 5. Photocatalytic degradation of DP over P25 and GOP composites under near-UV/Vis irradiation: influence of the (a) GO content and (b) temperature of treatment.

Figure 6. Total organic carbon (TOC) removal for DP and MO photocatalytic degradation under near-UV/Vis irradiation.

Figure 7. Photocatalytic degradation of MO over P25 and GOP composites under near-UV/Vis irradiation: influence of the (a) GO content and (b) temperature of treatment.

FIGURE 1

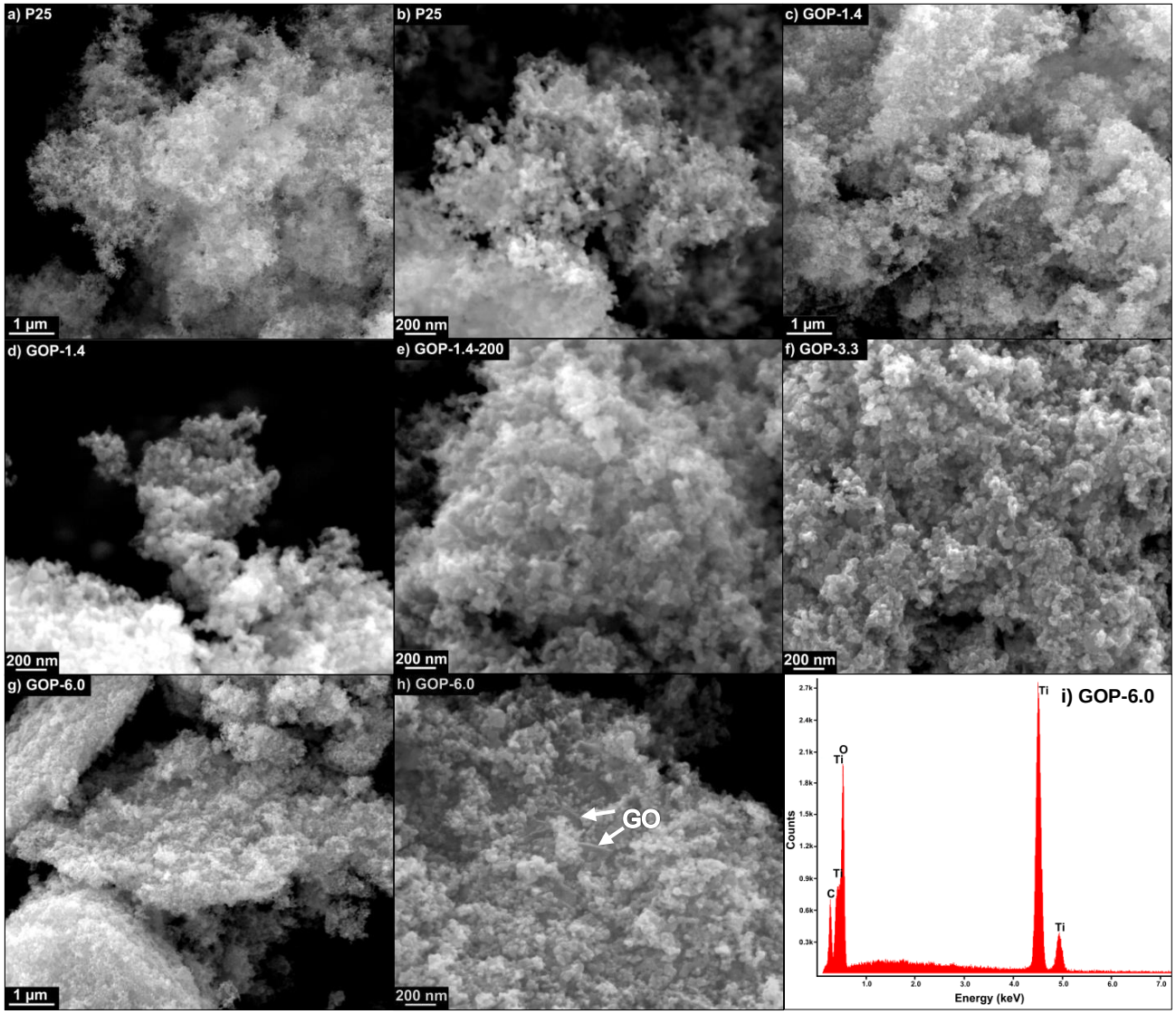
a) P25
1 µm
b) P25
200 nm
c) GOP-1.4
1 µm
d) GOP-1.4
200 nm
e) GOP-1.4-200
200 nm
f) GOP-3.3
200 nm
g) GOP-6.0
1 µm
h) GOP-6.0
GO
200 nm
i) GOP-6.0
Ti
O
Ti
Ti
C
Ti
Counts
Energy (keV)

FIGURE 2

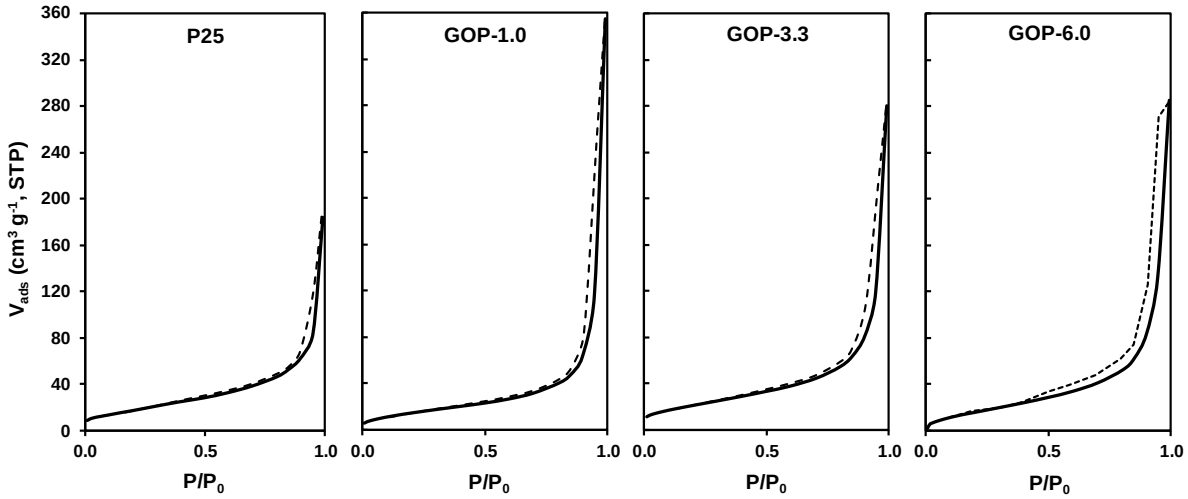
P25
GOP-1.0
GOP-3.3
GOP-6.0
V_{ads} (cm^3 g^{-1}, STP)
360
320
280
240
200
160
120
80
40
0
0.0
0.5
1.0
P/P$_0$

FIGURE 3

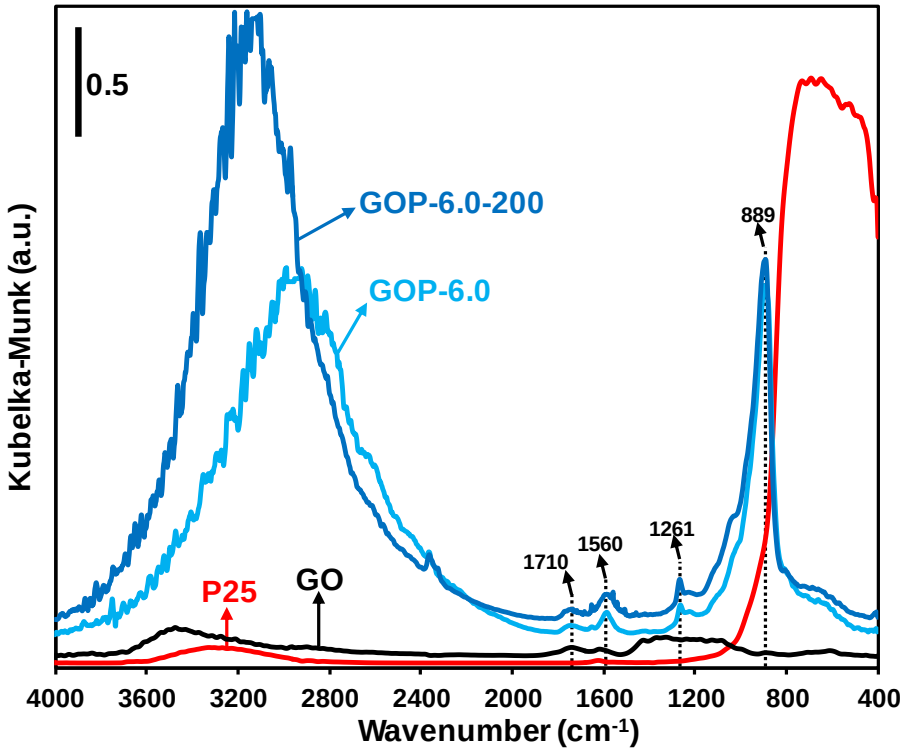
0.5
GOP-6.0-200
GOP-6.0
889
1261
1560
1710
P25
GO
Kubelka-Munk (a.u.)
4000
3600
3200
2800
2400
2000
1600
1200
800
400
Wavenumber (cm-1)

FIGURE 4

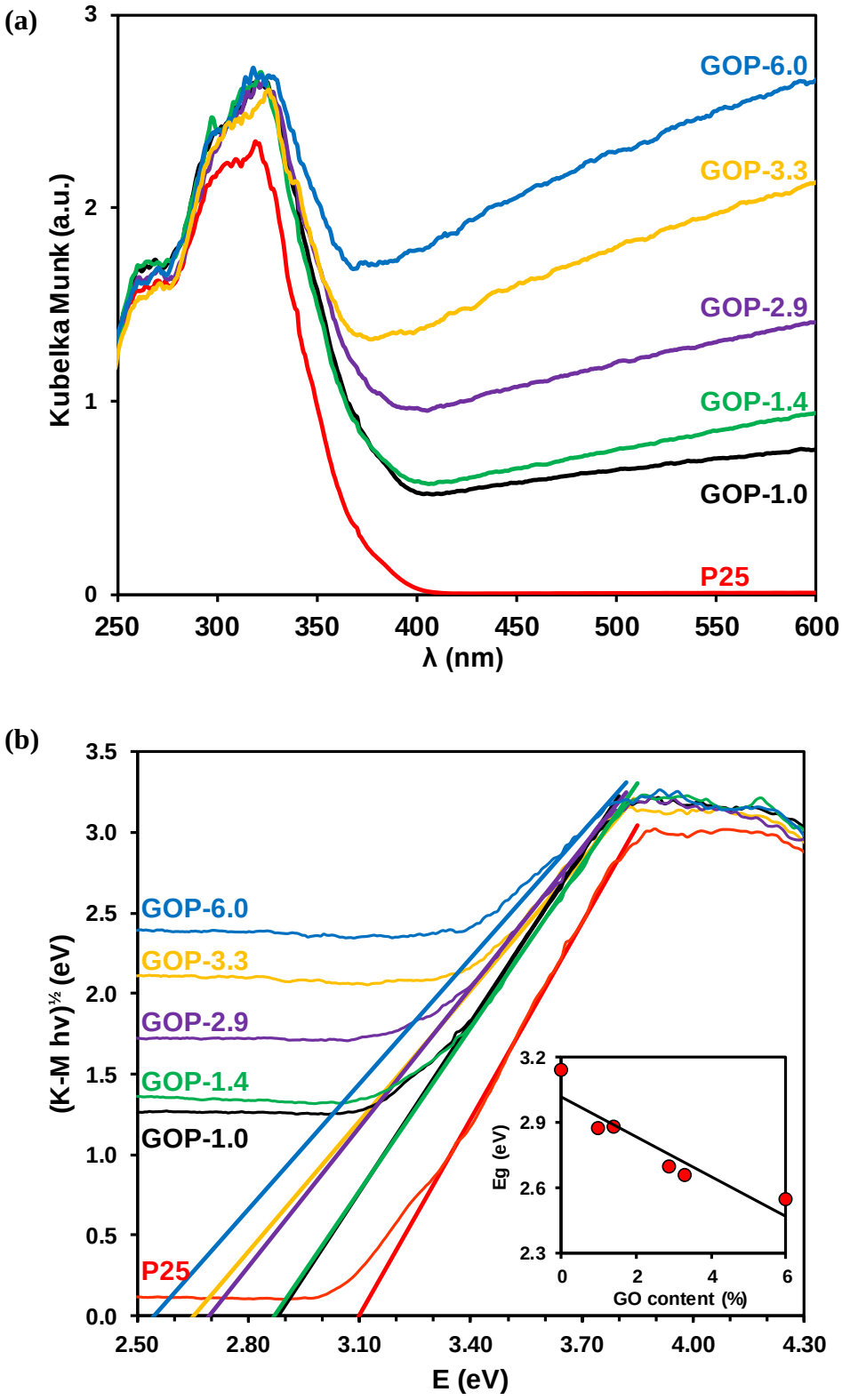
(a)
Kubelka Munk (a.u.)
λ (nm)
GOP-6.0
GOP-3.3
GOP-2.9
GOP-1.4
GOP-1.0
P25
(b)
(K-M hv)½ (eV)
E (eV)
Eg (eV)
GO content (%)

FIGURE 5

(a)

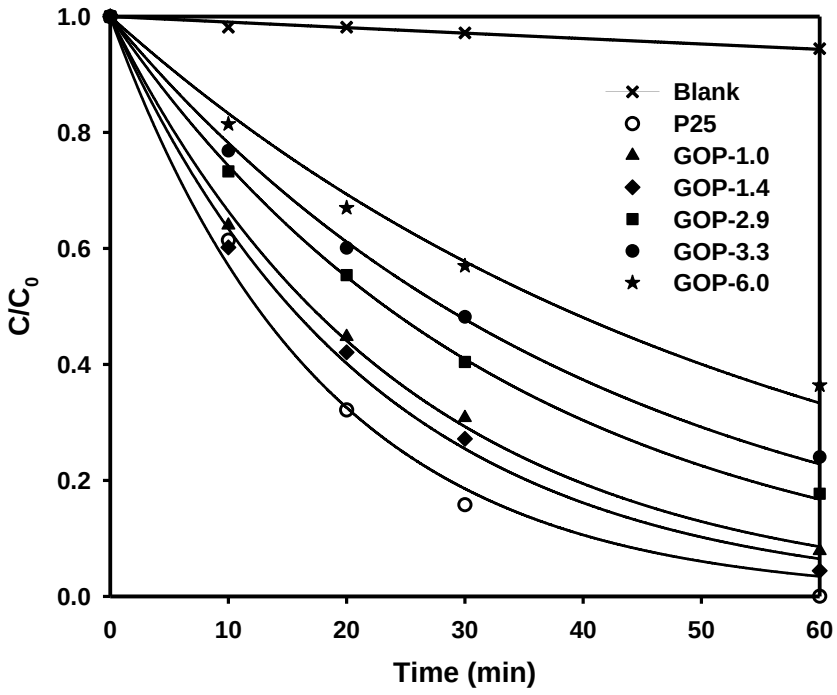
1.0
0.8
0.6
0.4
0.2
0.0
C/C0
0
10
20
30
40
50
60
Time (min)
Blank
P25
GOP-1.0
GOP-1.4
GOP-2.9
GOP-3.3
GOP-6.0

(b)

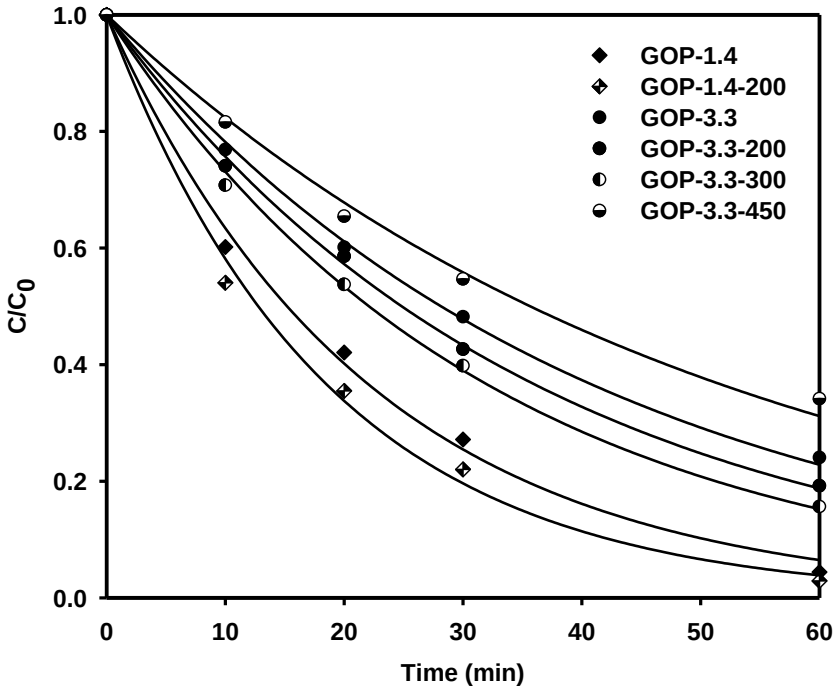
1.0
0.8
0.6
0.4
0.2
0.0
C/C0
0
10
20
30
40
50
60
Time (min)
GOP-1.4
GOP-1.4-200
GOP-3.3
GOP-3.3-200
GOP-3.3-300
GOP-3.3-450

FIGURE 6

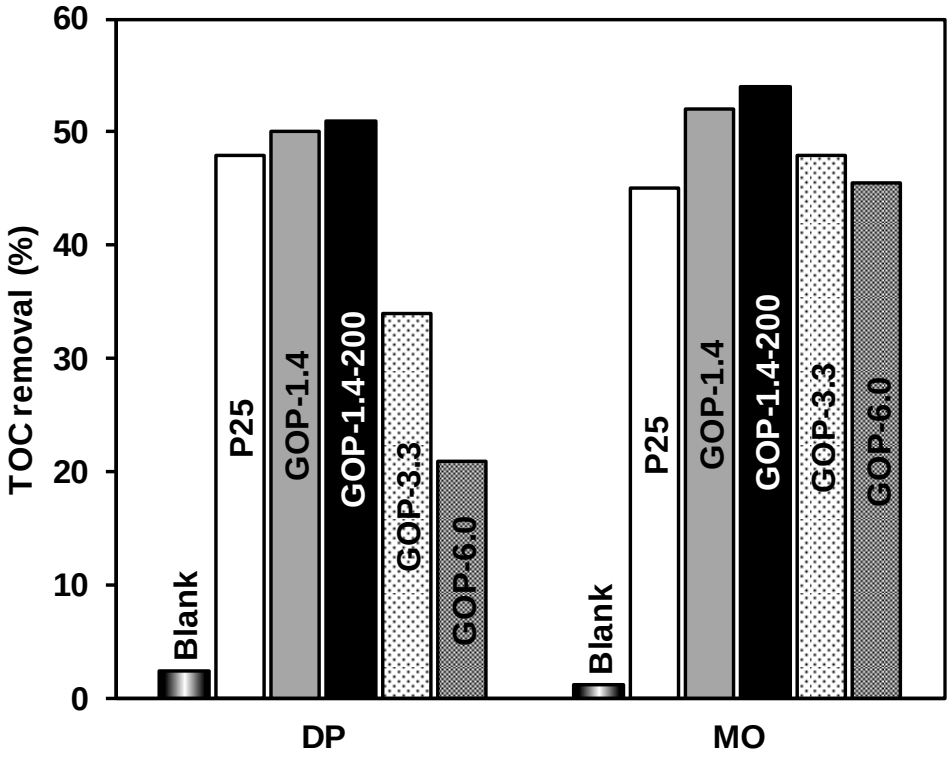
60
50
40
30
20
10
0
TOC removal (%)
Blank
P25
GOP-1.4
GOP-1.4-200
GOP-3.3
GOP-6.0
DP
MO

FIGURE 7

(a)

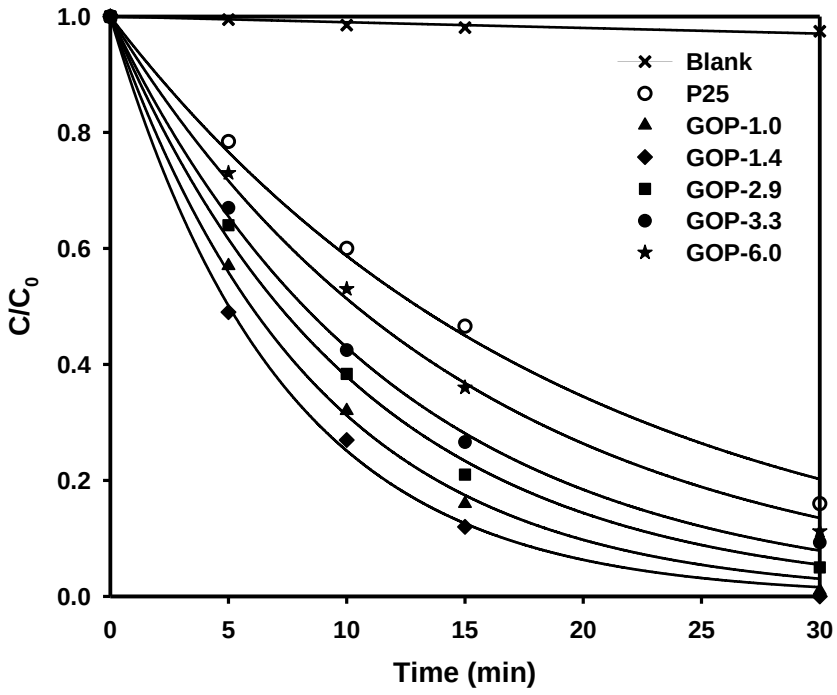
1.0
0.8
0.6
0.4
0.2
0.0
C/C0
0
5
10
15
20
25
30
Time (min)
Blank
P25
GOP-1.0
GOP-1.4
GOP-2.9
GOP-3.3
GOP-6.0

(b)

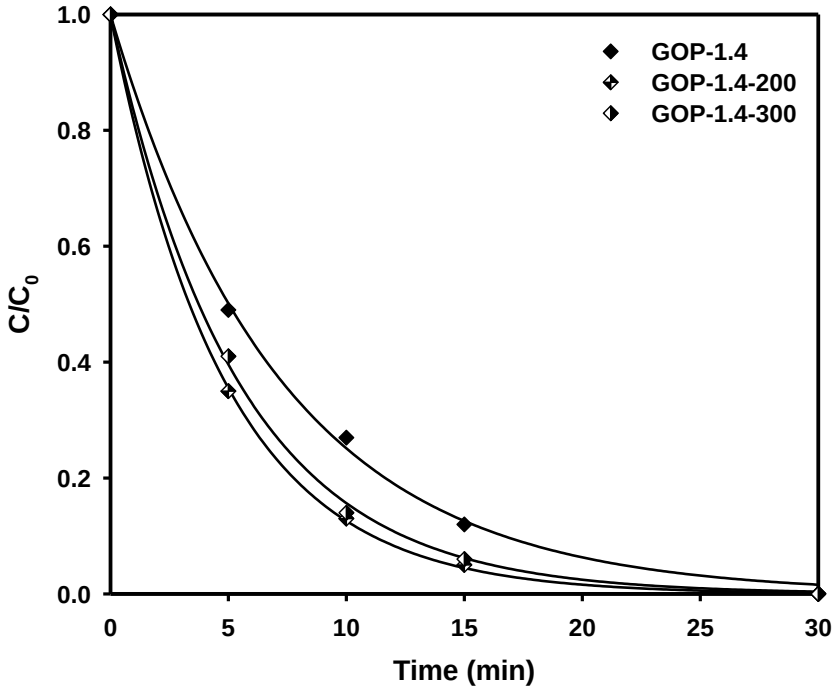
1.0
0.8
0.6
0.4
0.2
0.0
C/C0
0
5
10
15
20
25
30
Time (min)
GOP-1.4
GOP-1.4-200
GOP-1.4-300